Applied Catalysis B: Environmental 304 (2022) 120914

Contents lists available at ScienceDirect

Applied Catalysis B: Environmental

journal homepage: www.elsevier.com/locate/apcatb

Self-supported bimetallic phosphides with artificial heterointerfaces for enhanced electrochemical water splitting

Shuang Yang, Ji-Yu Zhu, Xiao-Nan Chen, Meng-Jie Huang, Sheng-Hao Cai, Ji-Yuan Han, Ji-Sen Li *

Department of Chemistry and Chemical Engineering, Jining University, Qufu 273155, China

ARTICLE INFO

Keywords:
Bimetallic phosphides
Heterojunctions
Hydrogen evolution reaction
Oxygen evolution reaction
Overall water splitting

ABSTRACT

Rational design and exploitation of efficient and inexpensive catalysts for water electrolysis are highly desired, yet very challenging. Herein, for the first time, we report a nanostructured catalyst of nickel phosphides-ruthenium phosphides self-supported on nickel foam (Ni_2P-Ru_2P/NF) through an in situ growth-phosphorization process. As expected, by virtue of prominent intrinsic activity, rich electrochemically active sites, and high electronic conductivity, the resultant Ni_2P-Ru_2P/NF exhibits enhanced electrocatalytic behavior for the oxygen evolution reaction and hydrogen evolution reaction, which delivers low overpotentials of 160 and 101 mV at 10 mA cm^{-2} in alkaline media, respectively. Remarkably, the Ni_2P-Ru_2P/NF can dramatically accelerate full water splitting with an ultralow cell voltage of 1.45 V at 10 mA cm^{-2}, which far exceeds the benchmark Pt-C/NF//RuO_2/NF (1.64 V) and ranks among the best electrocatalysts previously reported.

1. Introduction

To alleviate CO_2 emission and reduce fossil fuel consumption, it is of great urgency to explore green, clean, and sustainable energy sources [1,2]. Electrochemical water splitting, which can store electricity from intermittent energy in the form of molecular hydrogen, plays a crucial role in the development of hydrogen economy [3]. However, the hydrogen evolution reaction (HER) on the cathode is significantly limited by the anodic oxygen evolution reaction (OER), which involves kinetically sluggish process and requires a large overpotential, further reducing the efficiency of water electrolysis [4]. Although Pt-based nanomaterials and IrO_2/RuO_2 are considered to be high-performance electrocatalysts to accelerate H_2 and O_2 generation, respectively, their low abundance and prohibitive cost severely hamper the widespread application of electrolysis technology [5]. In this regard, rational design of high-performance and low-cost bifunctional electrocatalysts has become one of the hottest subjects in catalysis research, sparking more interest worldwide.

In recent years, tremendous efforts have been made to fabricate non-precious-metal-based catalysts, for instance, carbides [6–8], sulfides [9–11], etc.,[12,13] which can expedite water electrolysis efficiency and minimize the product cost. In particular, transition-metal phosphides (TMPs) with appealing electrocatalytic properties have been actively evaluated toward HER [14–18]. Simultaneously, recent researches also confirmed that TMPs-based nanomaterials can be employed for OER [19–21]. Despite significant progress, the electrocatalytic activities of most reported catalysts suffer from unsatisfactory electroactivity and are not superior to commercial Pt and IrO_2/RuO_2. Therefore, effective strategies are still highly desired to develop TMPs-based catalysts with high activity for electrochemical water splitting [22]. Among them, designing heterogeneous bimetallic phosphides or constructing heterointerfaces has been regarded as a paramount tool for enhancing electrocatalytic performance, which can generate abundant active sites, modulate electronic structure and improve conductivity [23–29]. At present, most nanostructured catalysts reported are powders, which are usually decorated on a current collector with the assistance of binders. Regrettably, the usage of polymer binders may result in some large drawbacks as follows: (1) increasing the contact resistance and inhibiting electrical conductivity [30]; (2) lower loading mass offers limited catalytic active sites by virtue of the weak adhesion between substrate and active species [31,32]; (3) nanoparticles are prone to aggregate and delaminate from the support during continuous operation process or high current electrolysis [33]. As a consequence, to address these issues, hybridizing heterostructured catalysts with conductive substrates is one of the most promising approaches [34–36], which can produce plentiful advantages including

* Corresponding author.
E-mail address: senjili@sina.com (J.-S. Li).

https://doi.org/10.1016/j.apcatb.2021.120914
Received 20 July 2021; Received in revised form 16 October 2021; Accepted 7 November 2021
Available online 15 November 2021

rapid charge transfer, excellent conductivity, and enhanced reaction kinetics.

Ruthenium (Ru) shows Pt-like catalytic properties, but it is markedly cheaper than Pt [21,37]. Especially, in recent years, ruthenium phosphides (RuP_x) have emerged as extraordinary electrocatalysts toward HER [38,39]. As well, RuP_x-based hybrids as OER catalysts have drawn considerable attention benefitting from the production of M-OH/M-O species on the surface of catalysts in water oxidation process [40–42], which can function as the real active sites. Given the above consideration, constructing an bifunctional catalyst of Ru-related bimetallic phosphides grown directly on conductive substrates is pivotal in boosting overall water splitting and has rarely been reported so far.

Herein, we demonstrate a simple and feasible route to prepare interface-rich nickel phosphides-ruthenium phosphides in-situ grown on nickel foam (Ni_2P-Ru_2P/NF) and investigated its electrochemical performance for the OER and HER. To our delight, thanks to the synergistic contribution and distinctive intrinsic activity, the resultant Ni_2P-Ru_2P/NF shows outstanding catalytic performance with small overpotentials of merely 160 and 101 mV to provide 10 mA cm^{-2} current density toward the OER and HER, respectively. Motivated by the superior OER and HER activities, a water electrolyzer comprising two pieces of Ni_2P-Ru_2P/NF only requires a low voltage of 1.45 V for driving 10 mA cm^{-2} with 15 h durability, far outperforming Pt-C/NF//RuO_2/NF electrolyzer.

2. Materials and methods

2.1. Chemicals

Ruthenium chloride hydrate ($RuCl_3{\cdot}xH_2O$), nitrate hexahydrate ($Ni(NO_3)_2{\cdot}6H_2O$), sodium dodecyl sulfate (SDS), ethylene glycol, potassium hydroxide (KOH), sodium hypophosphite monohydrate ($NaH_2PO_2{\cdot}H_2O$), and urea ($CO(NH_2)_2$) were afforded by Sinopharm Chemical Reagent Co., Ltd. Nafion (5.0 wt%) and iridium oxide (IrO_2) were obtained from Sigma-Aldrich. Commercial Pt/C (20 wt%) was purchased by Johnson Matthey. All chemicals were used as received.

2.2. Synthesis of NiRu-LDH on nickel foam (NF)

NiRu-LDH on NF was synthesized by a hydrothermal approach according to the previously reported literature [43]. Firstly, a NF (2 × 3 cm^2) was cleaned with ethanol, 1.0 M HCl aqueous solution, and deionized water for 10 min sequentially. Then, $Ni(NO_3)_2{\cdot}6H_2O$ (582 mg), $RuCl_3{\cdot}xH_2O$ (104 mg), SDS (144 mg) and urea (1 g) were dissolved in a mixture of deionized water (10 mL) and ethylene glycol (30 mL) via vigorously stirring, and then was added into Teflon autoclave. Next, the washed NF was transferred into the above solution and retained at 150 °C for 12 h. Finally, the sample was washed with methanol and deionized water in sequence, and dried at 60 °C for 5 h (named NiRu-LDH/NF). The Ni-LDH/NF was prepared without introducing $RuCl_3{\cdot}xH_2O$ with the same method.

2.3. Synthesis of Ni_2P- Ru_2P/NF

The as-prepared NiRu-LDH/NF and $NaH_2PO_2{\cdot}H_2O$ (50 mg) were placed at the downstream and upstream side of a tubular furnace, respectively. Then, the tubular furnace was heated to 350 °C and kept for 2 h under Ar. After natural cooling, the Ni_2P-Ru_2P/NF was achieved. The Ni_2P/NF was constructed using Ni-LDH/NF as precursor by the similar approach.

2.4. Preparation of IrO_2/NF and Pt-C/NF

A uniform ink was achieved utilizing commercial IrO_2 (20 mg) in a mixture of ethanol (1930 μL), and Nafion (70 μL), followed by sonication for 1.5 h (defined as IrO_2/NF). Thus, the ink was dropped on a pre-prepared NF (1 × 1 cm^2) and dried for 4 h. Similarly, the Pt-C electrode was also fabricated.

2.5. Instruments

Scanning electron microscopy (SEM) and corresponding energy dispersive X-ray spectroscopy (EDS) were operated on JSM-7800F. Transmission electron microscopy (TEM), and high-resolution (HR) TEM images were carried out using JEOL-2100 F. A D/max 2500/PC diffractometer (Cu Kα radiation) was utilized to obtain power X-ray diffraction (PXRD) patterns. Hydrophilic property was investigated via a Dataphysics-OCA100. X-ray photon spectroscopy (XPS) was taken on PHI 5000 Versa.

2.6. Electrochemical measurements

The OER and HER tests were conducted in 1.0 M KOH solution utilizing a typical three-electrode setup by an electrochemical station (CHI 760E), wherein Hg/HgO (1.0 M KOH), graphite rod, and the resulted catalysts self-supported NF (1 × 1 cm^2) were employed as the reference electrode, counter electrode, and working electrode, respectively. Noteworthily, the calibrated value for Hg/HgO is calculated to be about 0.924 V in 1.0 M KOH (Fig. S1), in which Pt wires were used as the counter and working electrode, respectively. All potentials were converted to the reversible hydrogen electrode (RHE): $E_{RHE} = 0.924\ V + E_{Hg/HgO}$. The OER and HER performance were examined by linear sweep voltammetry (LSV) at 2 mV s^{-1}. The electrochemical active surface area (ECSA) was investigated by cyclic voltammetry (CV) measurements with 20–100 mV s^{-1}. The full water splitting performance was assessed in a two-electrode system, where the resulted Ni_2P-Ru_2P/NF electrodes were chosen as anode and cathode, respectively. Additionally, the O_2 and H_2 produced were collected with a water drainage means.

3. Results and discussion

3.1. Materials synthesis and characterizations

As schematically depicted in Scheme 1, the Ni_2P-Ru_2P/NF electrode was prepared via a simple two-step strategy. In brief, commercial NF was chosen as the conductive support. Firstly, the NiRu-layered double hydroxide (NiRu LDH) was in situ grown on the NF through a hydrothermal procedure on the basis of the previously reported literature [43]. The scanning electron microscopy (SEM) images in Fig. S2 illustrate that the dense and stacked nanoparticles are uniformly distributed on NF with rich and open voids. Fig. S3 exhibits the powder X-ray diffraction (PXRD) pattern of the resultant sample, which was scraped off from NF. The diffraction peaks match well with the Bragg reflections of transition metal LDH framework [44]. Especially, the prominent peak at 14.9° is clearly discerned, which is characteristic of interlayered galleries. Thereafter, the as-prepared NiRu LDH can be transformed into Ni_2P-Ru_2P/NF after phosphorization treatment in Ar.

The crystal structure of Ni_2P-Ru_2P/NF was investigated by PXRD technique. As depicted in Fig. S4, the main peaks at 30.5°, 31.8°, 40.8°, 44.6°, 47.3°, 54.2°, 55.1°, 63.6°, 66.5°, 72.7°, and 74.9° correspond to the (110), (011), (111), (021), (210), (300), (211), (112), (202), (311), and (212) crystal faces of Ni_2P (JCPDS 65–3544), respectively. The other weak peaks are ascribed to Ru_2P (JCPDS 89–3031), indicative of lower crystallinity and small-sized nanoparticles in the hybrid [45]. As seen from Fig. 1a–c, the SEM images reveals that the resultant Ni_2P-Ru_2P/NF heterostructure remains the initial morphological feature of NiRu-LDH. The 3D porous structure is beneficial to enlarging contact with the electrolyte, facilitating mass transport, and expediting the release of gas bubbles during electrocatalytic process [19]. Moreover, the in situ production of Ni_2P-Ru_2P on the conductive NF can promote charge transfer and simultaneously prevent active centers from delaminating [27,31]. The energy dispersive X-ray spectroscopy (EDS) in Fig. S5

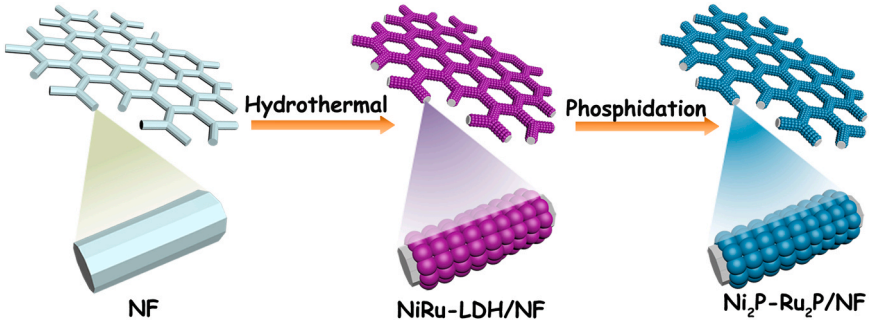

Scheme 1. Schematic illustration of the preparation of Ni_2P-Ru_2P/NF.

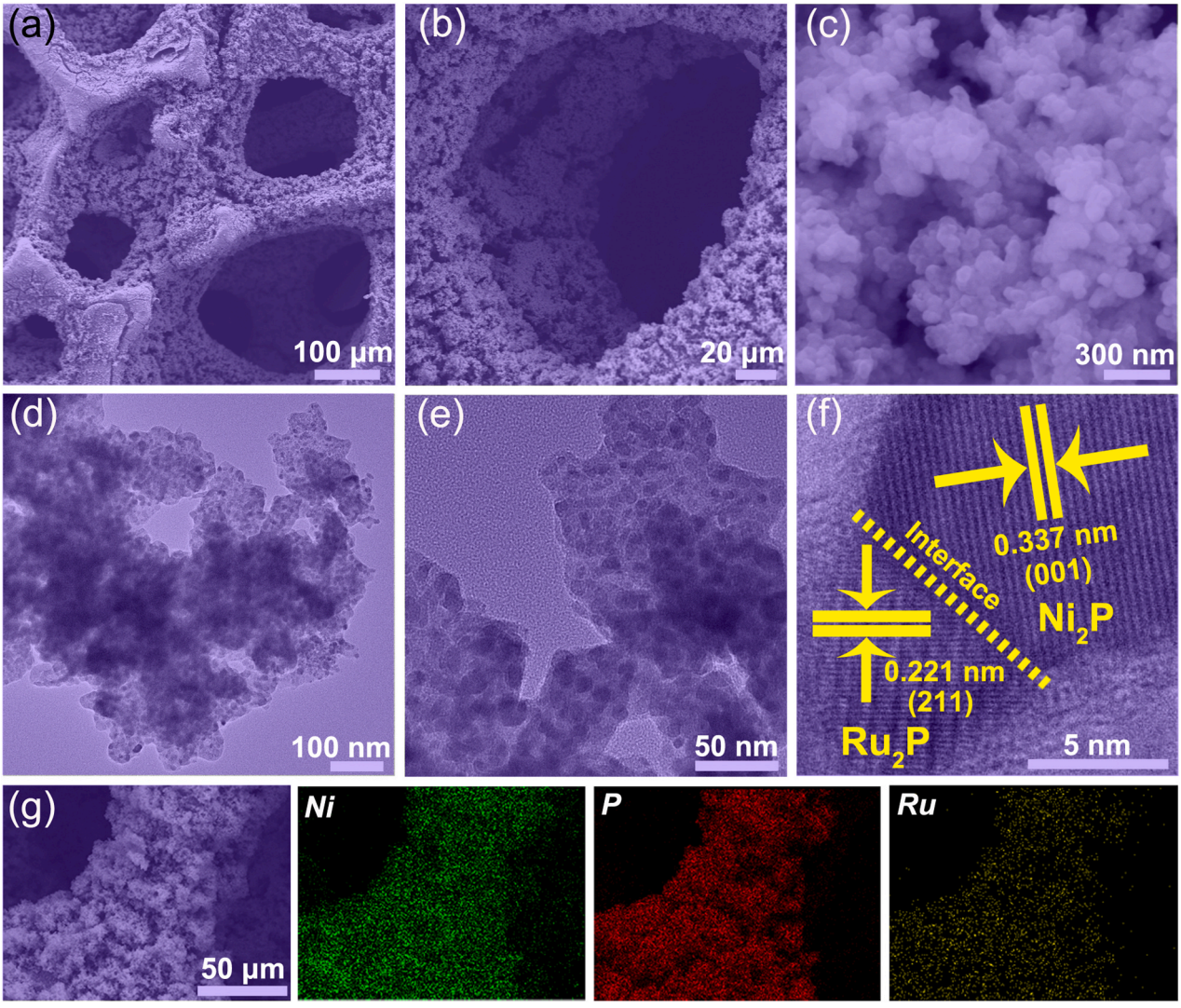

Fig. 1. (a–c) SEM, (d, e) TEM, (f) HRTEM, and (g) SEM of Ni_2P-Ru_2P/NF with the corresponding elemental mapping.

elucidates that the Ni_2P-Ru_2P/NF consists of Ni, Ru, and P elements. In Fig. 1d, e, the transmission electron microscopy (TEM) images demonstrate that the obtained hybrid is composed of abundant ultrasmall nanoparticles and amorphous nanodomains. Additionally, the high-resolution TEM image (Fig. 1f) strongly confirms the formation of heterojunction, and the interface between Ni_2P and Ru_2P labelled with yellow dotted line can be distinctly distinguished. Importantly, the heterostructure can result in an interfacial bonding effect and expose more active sites, thereby enhancing the catalytic performance [26,27]. The well-defined d-spacing of 0.337 and 0.221 nm are assigned to the (001) and (211) facets of Ni_2P and Ru_2P, respectively, in accordance with the XRD results. In addition, the homogeneous distribution of Ni, P, and Ru elements over the matrix is certified by the SEM and corresponding EDS elemental mapping images (Fig. 1g). As exhibited in Fig. S6, the contact angle for Ni_2P-Ru_2P/NF is 0° in comparison with NF (117.5°), reflecting that the resultant sample possesses a hydrophilic property. Noteworthily, the superhydrophilicity is conducive to maximizing the contact interface between the electrode and electrolyte and

rapidly releasing the gas bubbles formed in situ [27,46], thus contributing to high-performance catalytic activity and remarkable durability of the synthesized electrocatalysts.

For comparison, the Ni_2P /NF was prepared by the similar method yet in the absence of $RuCl_3$. The corresponding morphology and structure of the products were analyzed in detail and shown in Figs. S7–S10. In sharp contrast, it is found that numerous interconnected nanosheets were vertically grown on NF (Fig. S9). As revealed in Fig. S10, the characteristic diffraction peaks match well with hexagonal Ni_2P phase (JCPDS 65–3544).

The X-ray photoelectron spectroscopy (XPS) measurements were carried out to investigate the surface chemical composition and electronic state. As demonstrated in Fig. 2a, the XPS survey spectrum proves the presence of Ni, P, Ru, and O elements in Ni_2P-Ru_2P/NF. The high-resolution spectrum of Ni 2 P in Fig. 2b can be fitted into six peaks, which are attributed to Ni-P (853.3 and 870.5 eV), Ni-O (857.3 and 875.2 eV) and satellite peaks (861.5 and 880.2 eV), respectively [29]. Compared to that of Ni_2P/NF (Fig. S11), the Ni-P peak of Ni_2P-Ru_2P/NF shows a negative shift approximately 0.6 eV, strongly proving that the electron density of Ni species increased due to the addition of Ru^{3+} [9]. For the P 2p XPS spectrum in Fig. 2c, the binding energies at 129.4, and 130.3 eV correspond to the P $2p_{3/2}$ and P $2p_{1/2}$ of P 2p, further evidencing the generation of metal phosphides [40]. Particularly, a negative shift of 0.6 eV is seen for P $2p_{3/2}$ in comparison with elemental P (130.1 eV), representing the charge redistribution. The other at 134.4 eV is ascribed to P-O species. The appearance of Ni-O and P-O bonds should originate from inevitable surface oxidation [28]. As seen from Fig. 2d, the high-resolution Ru 3p spectrum shows two peaks located at 461.6 and 483.3 eV, which can be assignable to the Ru $3p_{3/2}$ and Ru $3p_{1/2}$ of in the Ru_2P [38,39]. The weak signal of Ru may be related to the low content of Ru in the resultant Ni_2P-Ru_2P/NF [47]. In view of the above-mentioned results, partial electrons transfer from Ni (Ru) to P could occur, beneficial to the enhancement of electrocatalytic HER performance [25].

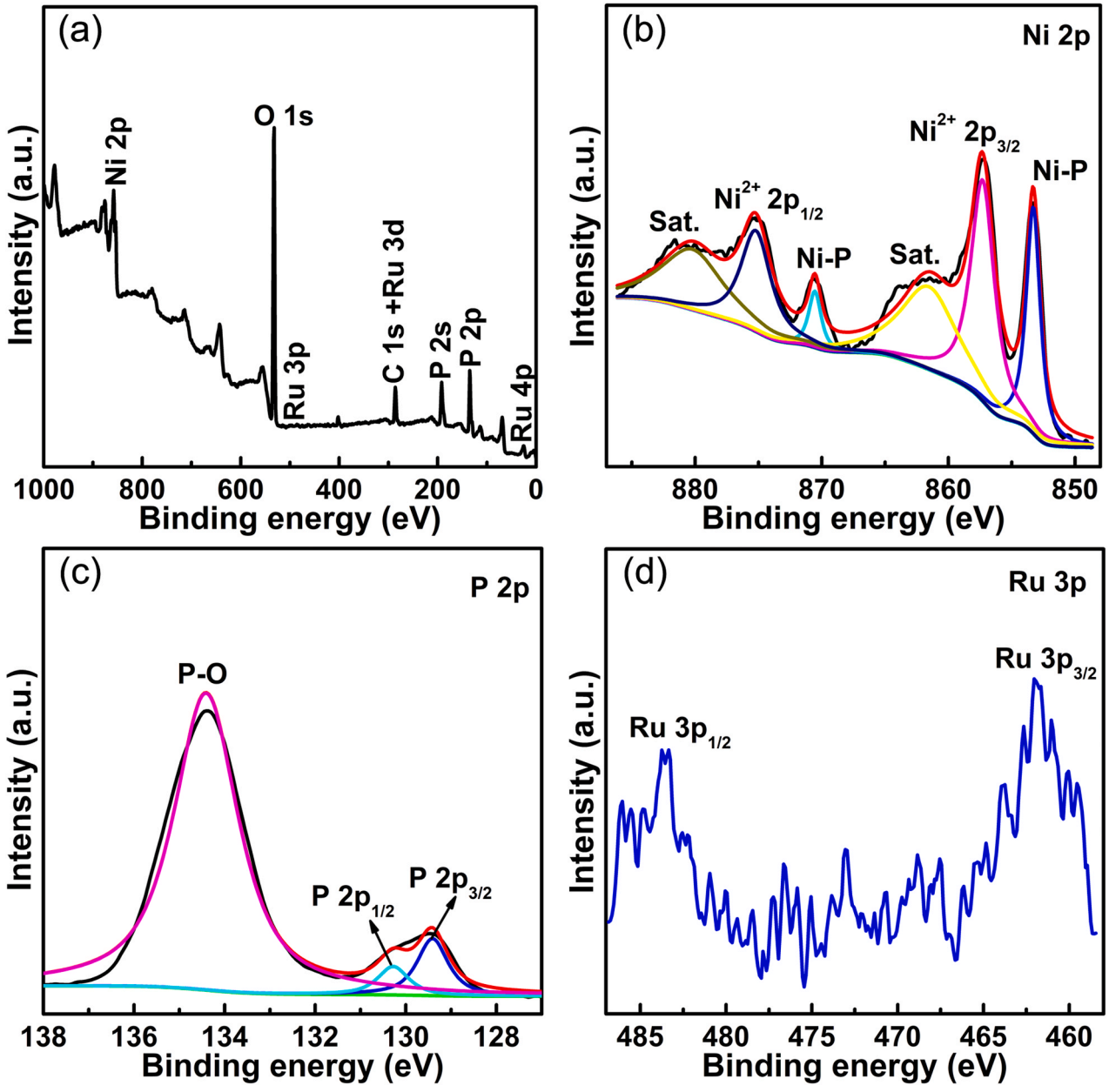

Fig. 2. (a) XPS survey spectrum, (b) Ni 2p, (c) P 2p, and (d) Ru 3p of Ni_2P-Ru_2P/NF.

3.2. Oxygen evolution reaction measurement

The electrocatalytic performance toward the OER of the as-fabricated samples were assessed in alkaline electrolytes (1.0 M KOH) with a representative three-electrode electrochemical configuration. To eliminate signal overlap between the OER and Ni^{2+}/Ni^{3+} oxidation, the polarization curves were carried out from high initial potential to low potential at 2 mV s^{-1}. For comparison, commercial IrO_2 coated on NF (IrO_2/NF) was also investigated. As depicted in linear sweep voltammetry (LSV) curves (Fig. 3a), the designed Ni_2P-Ru_2P/NF shows remarkable OER activity with an overpotential of merely 160 mV to offer 10 mA cm^{-2} current density, which is superior to Ni_2P/NF (210 mV) and IrO_2/NF (320 mV), confirming that the bimetallic phosphide heterostructure can be responsible for the greatly improved OER performance [26,39]. Remarkably, the catalytic behavior of Ni_2P-Ru_2P/NF is comparable, even superior to most of presently reported OER electrocatalytsts (Table S1) [14,24,28,48]. Additionally, to achieve a high current density of 100 mA cm^{-2}, an overpotential of only 258 mV is required (57 mV lower than that on Ni_2P /NF), suggesting the potential toward large-scale industrial applications (Fig. 3b). These results highlight that the prepared Ni_2P-Ru_2P/NF could function as high-performance OER catalysts under alkaline media. To investigate the intrinsic activity of electrocatalysts, the reaction kinetics were analyzed by the corresponding Tafel plots, shown in Fig. 3c. The Tafel slope of 41.5 mV dec^{-1} for Ni_2P-Ru_2P/NF is lower than those of Ni_2P/NF (49.9 mV dec^{-1}) and IrO_2/NF (101.5 mV dec^{-1}), significantly attesting that the introduction of Ru could effectively expedite the OER kinetics. Additionally, the double layer capacitance (C_{dl}) was tested to assess the electrochemical active surface area (ECSA) according to the corresponding cyclic voltammetry (CV) curves at different scan rates (20–100 mV s^{-1}). As presented in Figs. 3d and S12, the resultant Ni_2P-Ru_2P/NF possesses the larger C_{dl} value of 12.2 mF cm^{-2} compared to Ni_2P-Ru_2P/NF (6.1 mF cm^{-2}), implying the increase of exposed electroactive phases on the Ni_2P-Ru_2P heterojunction. Impressively, the higher intrinsic electroactivity toward the OER is reconfirmed by ECSA-normalized LSV curves in Fig. S13. As a consequence, such high intrinsic electroactivity and abundant catalytic active centers endow the designed Ni_2P-Ru_2P/NF electrode with extraordinary OER performance.

Apart from its pronounced catalytic behavior, long-term stability is also considerably crucial factor for practical applications of electrocatalysts. In Fig. 3e, it is found that the LSV curve of Ni_2P-Ru_2P/NF after 1000 cycles maintain almost unchanged in comparison with the initial one, implying its remarkable stability. Meanwhile, the durability of Ni_2P-Ru_2P/NF was further examined by chronopotentiometric measurement operated continuously at 1.49 V. As seen from Fig. 3f, 89% of the current density can be preserved after 10 h of consecutive electrolysis. Therefore, these results significantly manifest that the Ni_2P-Ru_2P/NF is a stable catalyst for the OER in alkaline condition, which should be ascribed to the intimate interaction of active nanomaterials and self-supporting conductive substrates without the assistance of binders [34]. Furthermore, the morphology, structure and composition of the post-OER Ni_2P-Ru_2P/NF were characterized by SEM, PXRD and XPS, respectively. As exhibited in Fig. S14, the SEM images reveal that the morphology is nearly identical to the initial. From the PXRD patterns (Fig. S15), the peaks corresponding to Ni_2P and Ru_2P decrease dramatically, while the new peaks of ruthenium and nickel oxides/oxyhydroxides can be clearly observed because of the partial oxidization in the range of OER potential [29]. Additionally, XPS was further carried out to probe the surface chemical state and composition after durability test. As shown in Fig. S16a, b, it is found that the peaks of Ni-P and Ru-P almost vanish, signifying that the metal phosphides may be oxidized to metal oxide/oxyhydroxide [19]. What's more, the result can be validated by the disappearance of the signal for P $2p_{3/2}$ (Fig. S16c) and the great decrease of P content from 20.07 to 0.69 atom%. On the basis of the above-mentioned results, we speculate that the actual active phases toward the OER should be in-situ formed oxides/oxyhydroxides in the oxygen evolution process.

3.3. Hydrogen evolution reaction measurement

In addition to electrocatalytic OER properties, the electrochemical HER activities of the as-synthesized Ni_2P-Ru_2P/NF were also measured in the same media. Ni_2P/NF and commercial 20% Pt-C loaded on bare NF (Pt-C/NF) were also assessed as reference. As displayed in Fig. 4a, the electroactivities of different electrodes follow the trend of Ni_2P/NF < Ni_2P-Ru_2P/NF < Pt-C/NF. Noticeably, the Ni_2P-Ru_2P/NF herorostructure demands a low overpotential of merely 101, 185, and 228 mV at 10, 100, and 200 mA cm^{-2} (Fig. 4b), respectively, which exceeds the Ni_2P/NF electrode (161, 253, and 292 mV) and most reported HER electrocatalysts so far (Table S2) [11,27,28]. The significant improvement of catalytic performance toward the HER may benefit from the powerful combination and effective synergistic effect between the Ni_2P-Ru_2P heterojunction and NF. In Fig. 4c, the Tafel slope of Ni_2P-Ru_2P/NF (56.7 mV dec^{-1}) is smaller than that of Ni_2P/NF (67.8 mV dec^{-1}), confirming the favorable kinetics with Volmer-Heyrovsky mechanism during the HER process [25,40]. Furthermore, the estimated C_{dl} for Ni_2P-Ru_2P/NF is about 27.7 mF cm^{-2}, 1.45 times higher than that of Ni_2P/NF (Figs. S17 and 4d). Importantly, on the basis of the LSV curves normalized by the ECSA, the Ni_2P-Ru_2P/NF still shows higher catalytic activity toward the HER in comparison with Ni_2P/NF (Fig. S18). Hence, these data undoubtedly confirm that the Ni_2P-Ru_2P heterostructure could effectively improve the intrinsic catalytic performance, thereby contributing prominent HER activity of Ni_2P-Ru_2P/NF. In addition, the stability of the as-prepared Ni_2P-Ru_2P/NF catalyst were evaluated by cycling test (Fig. 4e) and chronopotentiometry experiment (Fig. 4f), respectively. Surprisingly, negligible change and slight current decay can be observed. After HER test, the Ni_2P-Ru_2P/NF electrode exhibits no significant change (Figs. S19–S21), powerfully revealing its remarkable long-time durability for the HER.

As discussed above, the exceptional catalytic performance of the as-prepared Ni_2P-Ru_2P/NF toward the OER and HER could be assigned to the following factors: (1) The in situ formation of Ni_2P-Ru_2P heterojunction on conductive NF can not only offer a large surface area to disperse and stabilize active species, but also accelerate electron transport and enhance mechanical stability [31,49]. Especially, the hetero-interface of Ni_2P-Ru_2P is beneficial to generating numerous electroactive sites and unexpected synergistic contribution for the oxygen and hydrogen evolution [25]. (2) The hydrophilic surface characteristics assure intimate contact between electrolyte and active sites, thereby dramatically boosting the utilization efficiency of electroactive centers [46]. (3) 3D porous architecture can provide abundant channels to facilitate ion transfer and release of the bubbles produced throughout the water electrolysis, thus giving rise to boosted catalytic kinetics [35]. (4) The Ni_2P and Ru_2P are regarded as the real active phases for the HER [29], whereas their corresponding oxides and oxyhydroxide generated during the high electrode potential can function as catalytically active species toward the OER [40,41]. In short, these above merits collaboratively contribute to the unparalleled electrocatalytic properties toward the OER and HER in alkaline solutions.

3.4. Overall water-splitting measurement

Considering the prominent OER and HER performance, the resultant Ni_2P-Ru_2P/NF hybrid can work as a high-efficiency bifunctional electrocatalyst for overall water-splitting. Consequently, we further fabricated a two-electrode cell for water electrolysis utilizing two Ni_2P-Ru_2P/NF as both cathode and anode, as schematically shown in Fig. 5a. Intriguingly, plenty of vigorous O_2 and H_2 gas bubbles can be noticeably distinguished (Fig. 5b). As seen from the LSV curves (Fig. 5c), the Ni_2P-Ru_2P/NF electrode shows outstanding full water splitting behavior with a cell voltage of 1.45 V to obtain 10 mA cm^{-2} current density, which is

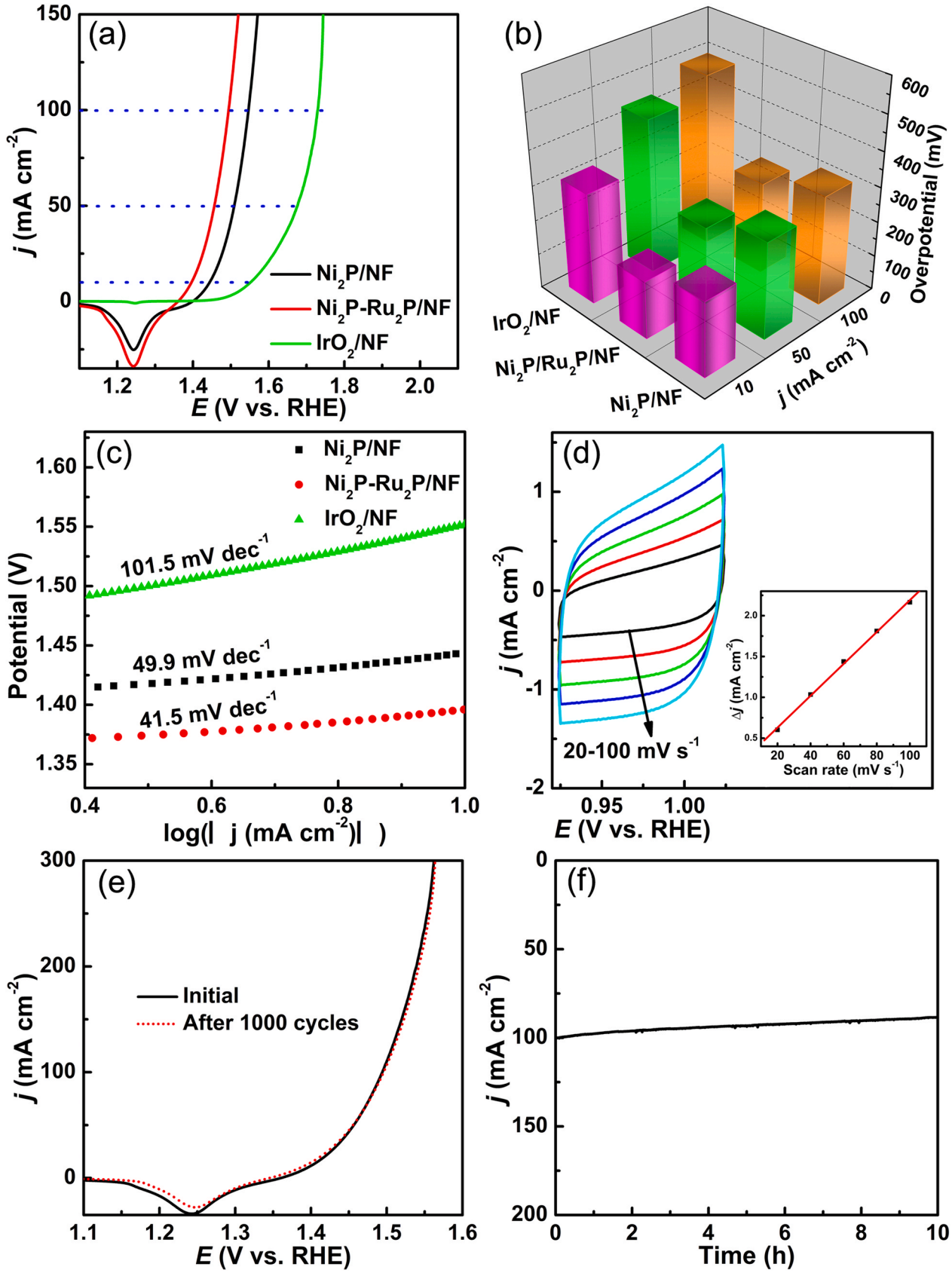

Fig. 3. Electrocatalytic performance of the electrodes for the OER. (a) LSV curves. (b) Comparison of overpotentials at 10, 50, and 100 mA cm^{-2}. (c) Tafel slopes. (d) CV curves under different scan rates in the region of 0.924–1.024 V. Inset: calculated C_{dl} for Ni_2P-Ru_2P/NF. (e) LSV curves of Ni_2P-Ru_2P/NF initial and after 1000 repetition cycles. (f) Chronopotentiometric measurement of Ni_2P-Ru_2P/NF at 1.49 V.

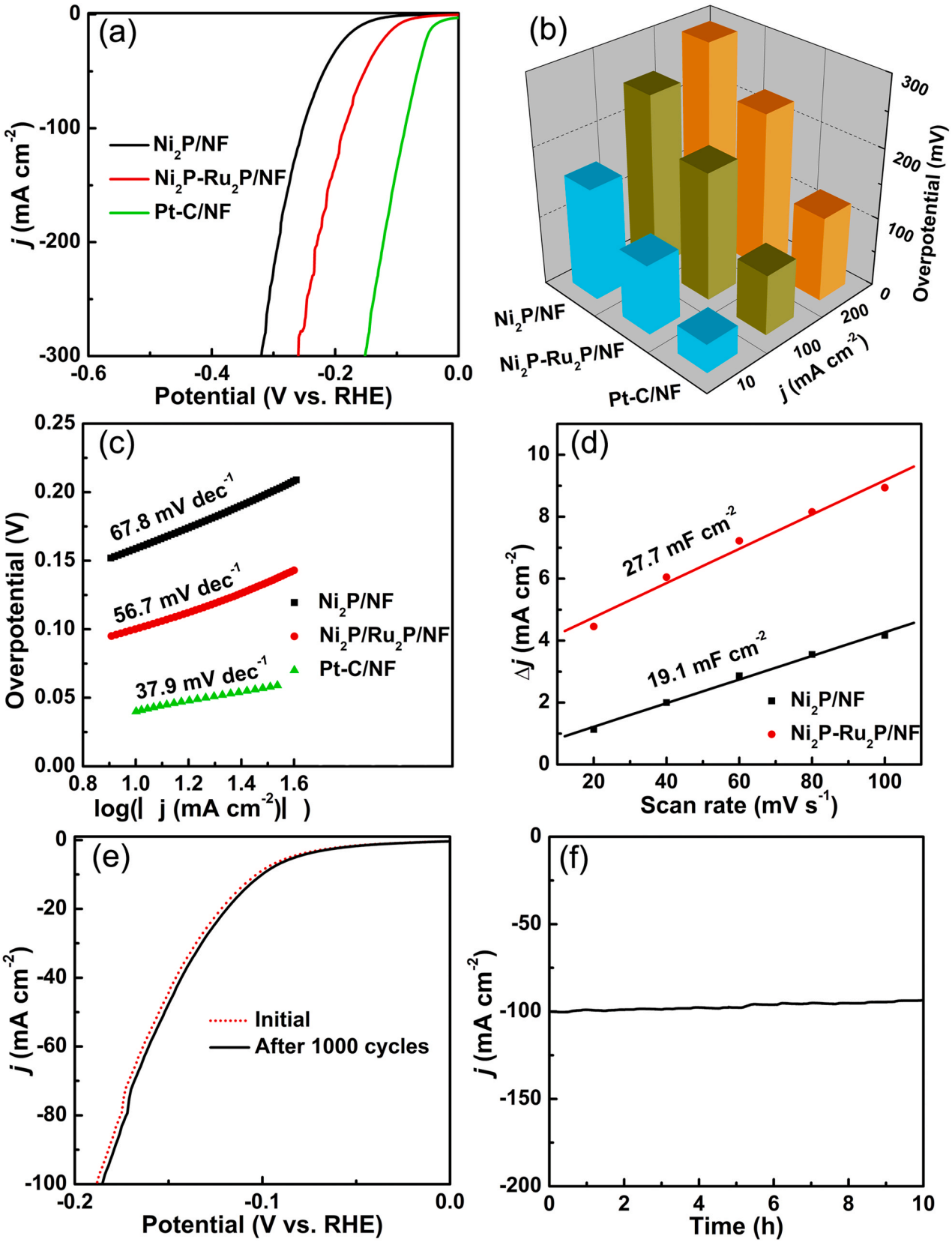

Fig. 4. Electrochemical activity of different catalysts toward the HER. (a) Polarization curves. (b) Comparison of corresponding overpotentials at 10, 100, and 200 mA cm^{-2}. (c) Tafel plots. (d) The plots of the current density against the scan rate. (e) LSV curves of Ni_2P-Ru_2P/NF initial and after 1000 CV cycles. (f) Chronopotentiometric response of Ni_2P-Ru_2P/NF at an overpotential of 185 mV.

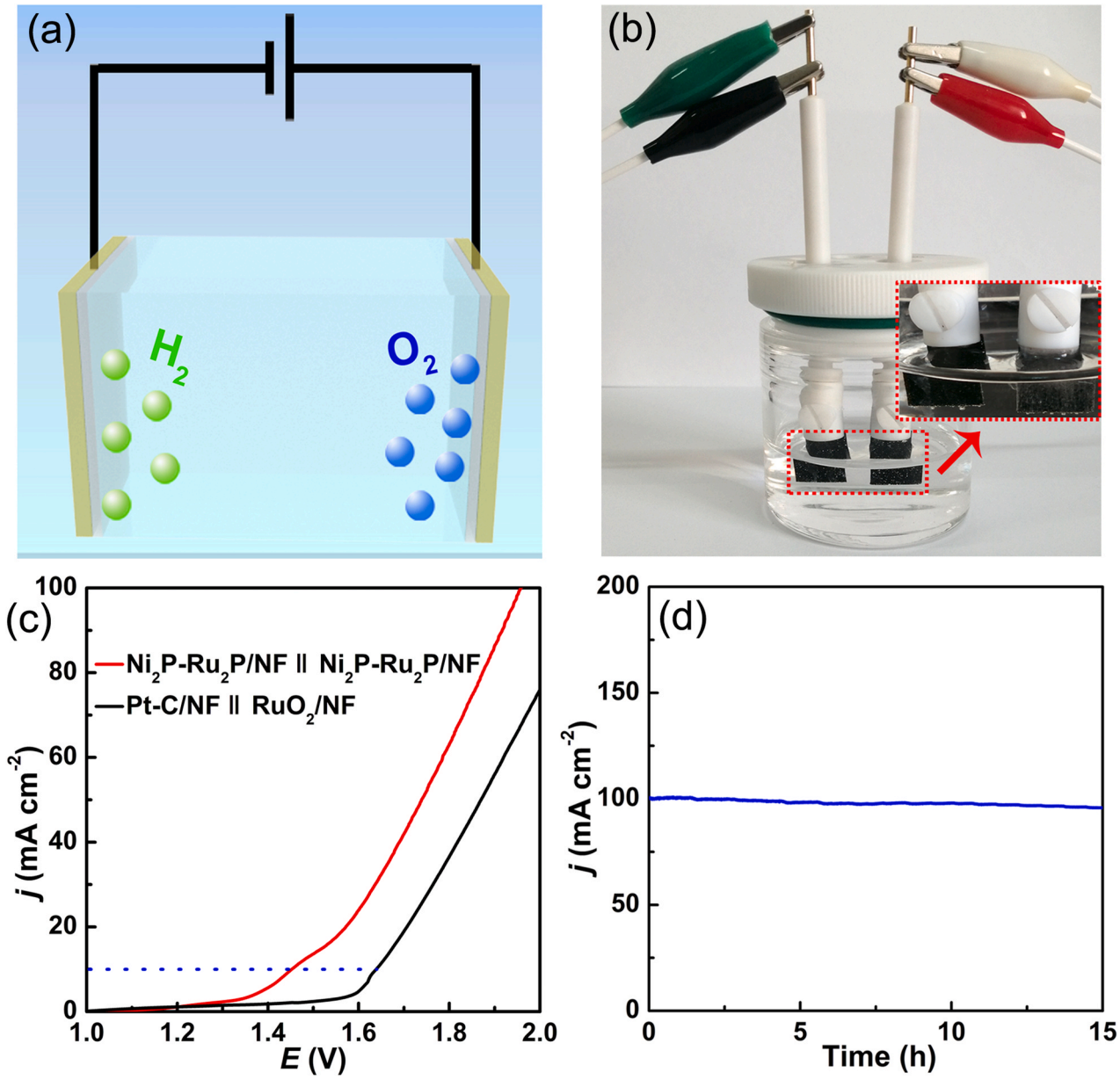

Fig. 5. (a) Schematic illustration of two-electrode cell. (b) Digital photograph of the fabricated two-electrode configuration for water splitting. (c) LSV curves of Ni_2P-Ru_2P/NF//Ni_2P-Ru_2P/NF and Pt-C/NF//RuO_2/NF electrodes. (d) Long-term durability test of Ni_2P-Ru_2P/NF//Ni_2P-Ru_2P/NF at 1.96 V.

superior to Pt-C/NF//RuO_2/NF (1.64 V) and many recently reported electrocatalysts (Table S3) [11,24,28]. After continuously operating for 15 h at 1.96 V (Fig. 5d), negligible current density decay can be discerned, suggesting the excellent stability for overall water-splitting.

Besides, the amounts of O_2 and H_2 produced in the H-type electrolytic apparatus, wherein the Ni_2P-Ru_2P/NF was employed as a catalyst, were measured by the water drainage approach (Fig. 6a–c), respectively. As exhibited in Fig. 6b, the electrolyzed water reaction container is separated with Nafion membrane. The sum of O_2 (H_2) generation at 0, 3, 6, 9, and 12 min can be intuitively observed (Fig. 6c). It is worth pointing out that the value of V_{O2}/V_{H2} is determined to be about 1:2 (Fig. 6d), which is consistent with the theoretically calculated value produced by water splitting, indicative of a Faradaic efficiency of approximately 100%. All in all, these results significantly corroborate that the as-designed Ni_2P-Ru_2P/NF is an efficient and durable catalyst for the water electrolysis.

4. Conclusions

In summary, we have elaborately explored a Ni_2P-Ru_2P heterojunction grown directly on NF through a facile hydrothermal-phosphorization strategy for the first time. The resultant Ni_2P-Ru_2P/NF electrode as bifunctional electrocatalyst reveals substantially enhanced catalytic performance with lower overpotentials, smaller Tafel slopes, along with long-term durability toward the OER and HER, respectively, which is associated to the synergy of different component and unique structural feature. Surprisingly, a full electrolyzer is capable of delivering 10 mA cm^{-2} with a lower cell voltage of 1.45 V and can operate well for at least 15 h, far excelling Pt-C/NF//RuO_2/NF (1.64 V). More importantly, this proposed synthetic approach can also be adopted to design high-efficiency bimetallic phosphides-based catalysts for electrocatalytic applications.

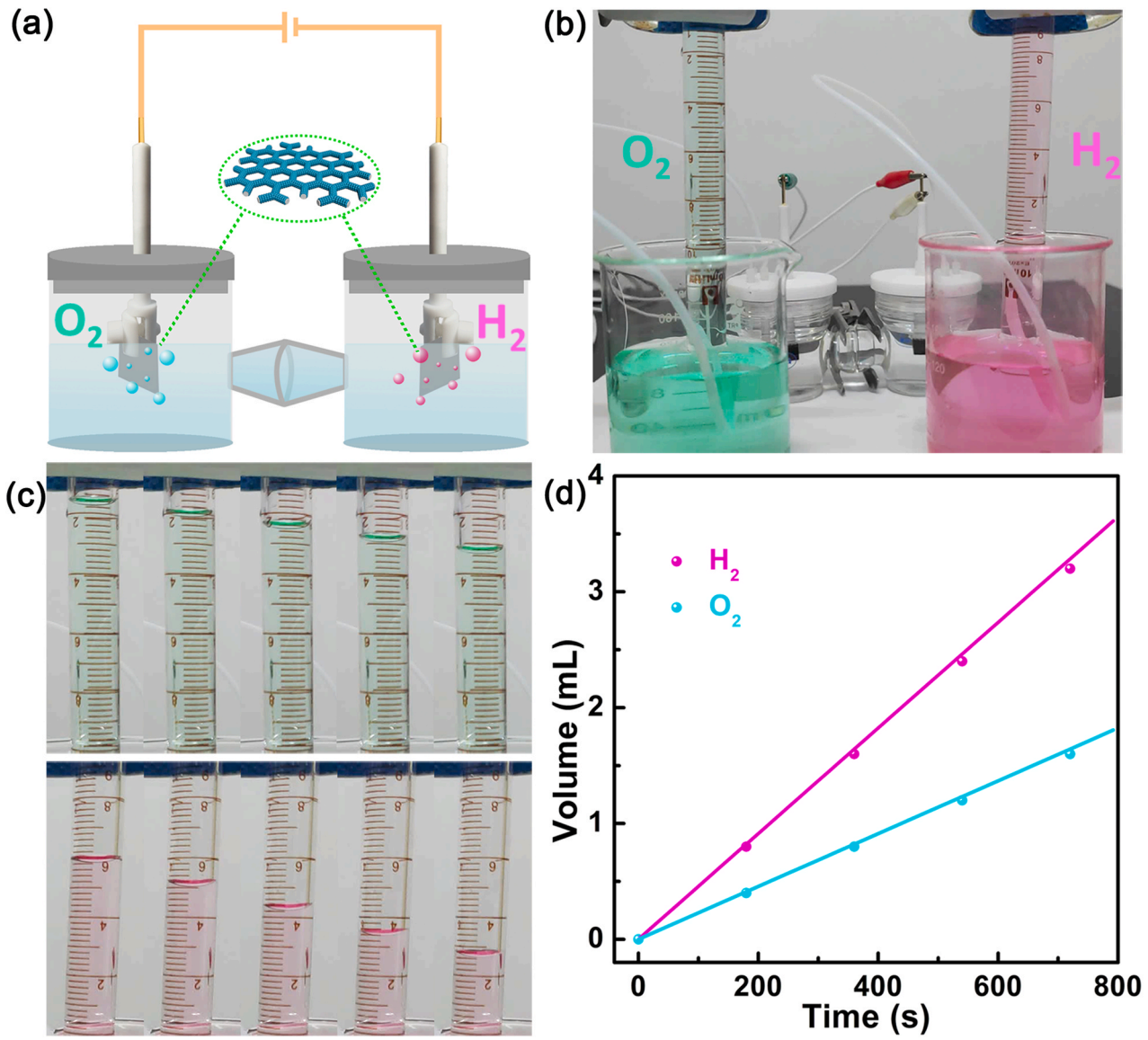

Fig. 6. (a) Schematic of the electrolyzed water reaction. (b) Digital photograph of gas collection device for water splitting. (c) Oxygen and hydrogen generated at 0, 3, 6, 9, and 12 min (d) Amount of O_2 and H_2 as function of time.

CRediT authorship contribution statement

Shuang Yang: Conceptualization, Data curation, Writing – original draft. **Ji-Yu Zhu:** Resources, Methodology. **Xiao-Nan Chen:** Resources, Methodology. **Meng-Jie Huang:** Data curation. **Sheng-Hao Cai:** Data curation. **Ji-Yuan Han:** Data curation, Validation. **Ji-Sen Li:** Conceptualization, Funding acquisition, Supervision, Writing – review & editing.

Declaration of Competing Interest

The authors declare that they have no known competing financial interests or personal relationships that could have appeared to influence the work reported in this paper.

Acknowledgements

This work was financially supported by the National Natural Science Foundation of China (No. 21971086) and the Natural Science Foundation of Shandong Province (No. ZR2019MB013).

Appendix A. Supporting information

Supplementary data associated with this article can be found in the online version at doi:10.1016/j.apcatb.2021.120914.

References

[1] J.A. Turner, Sustainable hydrogen production, Science 305 (2004) 972–974, https://doi.org/10.1126/science.1103197.
[2] Z. Wu, Y. Zhao, W. Jin, B. Jia, J. Wang, T. Ma, Recent progress of vacancy engineering for electrochemical energy conversion related applications, Adv. Funct. Mater. 31 (2021), 2009070, https://doi.org/10.1002/adfm.202009070.
[3] J. Zhu, L. Hu, P. Zhao, L.Y.S. Lee, K.-Y. Wong, Recent advances in electrocatalytic hydrogen evolution using nanoparticles, Chem. Rev. 120 (2020) 851–918, https://doi.org/10.1021/acs.chemrev.9b00248.
[4] M.G. Walter, E.L. Warren, J.R. McKone, S.W. Boettcher, Q. Mi, E.A. Santori, N. S. Lewis, Solar water splitting cells, Chem. Rev. 110 (2010) 6446–6473, https://doi.org/10.1021/cr1002326.
[5] Y. Jiao, Y. Zheng, M. Jaroniec, S.Z. Qiao, Design of electrocatalysts for oxygen- and hydrogen-involving energy conversion reactions, Chem. Soc. Rev. 44 (2015) 2060–2086, https://doi.org/10.1039/C4CS00470A.
[6] J.-S. Li, Y. Wang, C.-H. Liu, S.-L. Li, Y.-G. Wang, L.-Z. Dong, Z.-H. Dai, Y.-F. Li, Y.-Q. Lan, Coupled molybdenum carbide and reduced graphene oxide electrocatalysts for efficient hydrogen evolution, Nat. Commun. 7 (2016) 11204, https://doi.org/10.1038/ncomms11204.

[7] Z. Kou, T. Wang, Q. Gu, M. Xiong, L. Zheng, X. Li, Z. Pan, H. Chen, F. Verpoort, A. K. Cheetham, S. Mu, J. Wang, Rational design of holey 2D nonlayered transition metal carbide/nitride heterostructure nanosheets for highly efficient water oxidation, Adv. Energy Mater. 9 (2019), 1803768, https://doi.org/10.1002/aenm.201803768.

[8] T. Gu, R. Sa, L. Zhang, D.-S. Li, R. Wang, Engineering interfacial coupling between Mo_2C nanosheets and Co@NC polyhedron for boosting electrocatalytic water splitting and zinc-air batteries, Appl. Catal. B Environ. 296 (2021), 120360, https://doi.org/10.1016/j.apcatb.2021.120360.

[9] J. Sun, H. Xue, N. Guo, T. Song, Y.-r Hao, J. Sun, J. Zhang, Q. Wang, Synergetic metal defect and surface chemical reconstruction into NiCo2S4/ZnS heterojunction to achieve outstanding oxygen evolution performance, Angew. Chem. Int. Ed. 60 (2021) 19435–19441, https://doi.org/10.1002/anie.202107731.

[10] Y. Li, M.B. Majewski, S.M. Islam, S. Hao, A.A. Murthy, J.G. DiStefano, E.D. Hanson, Y. Xu, C. Wolverton, M.G. Kanatzidis, M.R. Wasielewski, X. Chen, V.P. Dravid, Morphological engineering of winged Au@MoS_2 heterostructures for electrocatalytic hydrogen evolution, Nano Lett. 18 (2018) 7104–7110, https://doi.org/10.1021/acs.nanolett.8b03109.

[11] Y. Yang, H. Yao, Z. Yu, S.M. Islam, H. He, M. Yuan, Y. Yue, K. Xu, W. Hao, G. Sun, H. Li, S. Ma, P. Zapol, M.G. Kanatzidis, Hierarchical nanoassembly of MoS_2/Co_9S_8/Ni_3S_2/Ni as a highly efficient wide-pH range electrocatalyst for overall water splitting, J. Am. Chem. Soc. 141 (2019) 10417, https://doi.org/10.1021/jacs.9b04492.

[12] Y. Liu, Q. Feng, W. Liu, Q. Li, Y. Wang, B. Liu, L. Zheng, W. Wang, L. Huang, L. Chen, X. Xiong, Y. Lei, Boosting interfacial charge transfer for alkaline hydrogen evolution via rational interior Se modification, Nano Energy 81 (2021), 105641, https://doi.org/10.1016/j.nanoen.2020.105641.

[13] C. Huang, B. Zhang, Y. Wu, Q. Ruan, L. Liu, J. Su, Y. Tang, R. Liu, P.K. Chu, Experimental and theoretical investigation of reconstruction and active phases on honeycombed Ni_3N-Co_3N/C in water splitting, Appl. Catal. B Environ. 297 (2021), 120461, https://doi.org/10.1016/j.apcatb.2021.120461.

[14] Z. Pu, T. Liu, I.S. Amiinu, R. Cheng, P. Wang, C. Zhang, P. Ji, W. Hu, J. Liu, S. Mu, Transition-metal phosphides: activity origin, energy-related electrocatalysis applications, and synthetic strategies, Adv. Funct. Mater. 30 (2020), 2004009, https://doi.org/10.1002/adfm.202004009.

[15] Y.-J. Tang, H.-J. Zhu, L.-Z. Dong, A.M. Zhang, S.-L. Li, J. Liu, Y.-Q. Lan, Solid-phase hot-pressing of POMs-ZIFs precursor and derived phosphide for overall water splitting, Appl. Catal. B Environ. 245 (2019) 528–535, https://doi.org/10.1016/j.apcatb.2019.01.007.

[16] Z. Pu, J. Zhao, I.S. Amiinu, W. Li, M. Wang, D. He, S. Mu, A universal synthesis strategy for P-rich noble metal diphosphide-based electrocatalysts for the hydrogen evolution reaction, Energy Environ. Sci. 12 (2019) 952, https://doi.org/10.1039/C9EE00197B.

[17] Y. Zhao, N. Jia, X.-R. Wu, F.-M. Li, P. Chen, P.-J. Jin, S. Yin, Y. Chen, Rhodium phosphide ultrathin nanosheets for hydrazine oxidation boosted electrochemical water splitting, Appl. Catal. B Environ. 270 (2020), 118880, https://doi.org/10.1016/j.apcatb.2020.118880.

[18] S. Riyajuddin, K. Azmi, M. Pahuja, S. Kumar, T. Maruyama, C. Bera, K. Ghosh, Super-hydrophilic hierarchical Ni-foam-graphene-carbon nanotubes-Ni_2P–CuP_2 nano-architecture as efficient electrocatalyst for overall water splitting, ACS Nano 15 (2021) 5586–5599, https://doi.org/10.1021/acsnano.1c00647.

[19] S. Sun, X. Zhou, B. Cong, W. Hong, G. Chen, Tailoring the d-band centers endows $(Ni_xFe_{1-x})_2P$ nanosheets with efficient oxygen evolution catalysis, ACS Catal. 10 (2020) 9086–9097, https://doi.org/10.1021/acscatal.0c01273.

[20] B. Qiu, L. Cai, Y. Wang, Z. Lin, Y. Zuo, M. Wang, Y. Chai, Fabrication of nickel–cobalt bimetal phosphide nanocages for enhanced oxygen evolution catalysis, Adv. Funct. Mater. 28 (2018), 1706008, https://doi.org/10.1002/adfm.201706008.

[21] C.-B. Hong, X. Li, W.-B. Wei, X.-T. Wu, Q.-L. Zhu, Nano-engineering of Ru-based hierarchical porous nanoreactors for highly efficient pH-universal overall water splitting, Appl. Catal. B Environ. 294 (2021), 120230, https://doi.org/10.1016/j.apcatb.2021.120230.

[22] H. Zhang, A.W. Maijenburg, X. Li, S.L. Schweizer, R.B. Wehrspohn, Bifunctional heterostructured transition metal phosphides for efficient electrochemical water splitting, Adv. Funct. Mater. 30 (2020), 2003261, https://doi.org/10.1002/adfm.202003261.

[23] D. Chen, R. Lu, Z. Pu, J. Zhu, H.-W. Li, F. Liu, S. Hu, X. Luo, J. Wu, Y. Zhao, S. Mu, Ru-doped 3D flower-like bimetallic phosphide with a climbing effect on overall water splitting, Appl. Catal. B Environ. 279 (2020), 119396, https://doi.org/10.1016/j.apcatb.2020.119396.

[24] X. Luo, P. Ji, P. Wang, R. Cheng, D. Chen, C. Lin, J. Zhang, J. He, Z. Shi, N. Li, S. Xiao, S. Mu, Interface engineering of hierarchical branched Mo-doped Ni_3S_2/Ni_xP_y hollow heterostructure nanorods for efficient overall water splitting, Adv. Energy Mater. 10 (2020), 1903891, https://doi.org/10.1002/aenm.201903891.

[25] A. Kumar, V.Q. Bui, J. Lee, A.R. Jadhav, Y. Hwang, M.G. Kim, Y. Kawazoe, H. Lee, Modulating interfacial charge density of NiP_2–FeP_2 via coupling with metallic Cu for Accelerating alkaline hydrogen evolution, ACS Energy Lett. 6 (2021) 354–363, https://doi.org/10.1021/acsenergylett.0c02498.

[26] H. Yan, Y. Xie, A. Wu, Z. Cai, L. Wang, C. Tian, X. Zhang, H. Fu, Anion-modulated HER and OER activities of 3D Ni-V-based interstitial compound heterojunctions for high-efficiency and stable overall water splitting, Adv. Mater. 31 (2019), 1901174, https://doi.org/10.1002/adma.201901174.

[27] L. Wu, L. Yu, F. Zhang, B. McElhenny, D. Luo, A. Karim, S. Chen, Z. Ren, Heterogeneous bimetallic phosphide Ni_2P-Fe_2P as an efficient bifunctional catalyst for water/seawater splitting, Adv. Funct. Mater. 31 (2021), 2006484, https://doi.org/10.1002/adfm.202006484.

[28] J. Wang, M. Zhang, G. Yang, W. Song, W. Zhong, X. Wang, M. Wang, T. Sun, Y. Tang, Heterogeneous bimetallic Mo-NiP_x/NiS_y as a highly efficient electrocatalyst for robust Overall water splitting, Adv. Funct. Mater. 31 (2021), 2101532, https://doi.org/10.1002/adfm.202101532.

[29] F. Yu, H. Zhou, Y. Huang, J. Sun, F. Qin, J. Bao, W.A. Goddard, S. Chen, Z. Ren, High-performance bifunctional porous non-noble metal phosphide catalyst for overall water splitting, Nat. Commun. 9 (2018) 2551, https://doi.org/10.1038/s41467-018-04746-z.

[30] C. Xia, Q. Jiang, C. Zhao, M.N. Hedhili, H.N. Alshareef, Selenide-based electrocatalysts and scaffolds for water oxidation applications, Adv. Mater. 28 (2016) 77–85, https://doi.org/10.1002/adma.201503906.

[31] H. Sun, Z. Yan, F. Liu, W. Xu, F. Cheng, J. Chen, Self-supported transition-metal-based electrocatalysts for hydrogen and oxygen evolution, Adv. Mater. 32 (2020), 1806326, https://doi.org/10.1002/adma.201806326.

[32] Y.-L. Wu, X. Li, Y.-S. Wei, Z. Fu, W. Wei, X.-T. Wu, Q.-L. Zhu, Q. Xu, Ordered macroporous superstructure of nitrogen-doped nanoporous carbon implanted with ultrafine Ru nanoclusters for efficient pH-universal hydrogen evolution reaction, Adv. Mater. 33 (2021), 2006965, https://doi.org/10.1002/adma.202006965.

[33] Y. Chen, G. Yu, W. Chen, Y. Liu, G.-D. Li, P. Zhu, Q. Tao, Q. Li, J. Liu, X. Shen, H. Li, X. Huang, D. Wang, T. Asefa, X. Zou, Highly active, nonprecious electrocatalyst comprising borophene subunits for the hydrogen evolution reaction, J. Am. Chem. Soc. 139 (2017) 12370–12373, https://doi.org/10.1021/jacs.7b06337.

[34] J. Hou, Y. Wu, B. Zhang, S. Cao, Z. Li, L. Sun, Rational design of nanoarray architectures for electrocatalytic water splitting, Adv. Funct. Mater. 29 (2019), 1808367, https://doi.org/10.1002/adfm.201808367.

[35] J. Liu, D. Zhu, Y. Zheng, A. Vasileff, S.-Z. Qiao, Self-supported earth-abundant nanoarrays as efficient and robust electrocatalysts for energy-related reactions, ACS Catal. 8 (2018) 6707–6732, https://doi.org/10.1021/acscatal.8b01715.

[36] Y. Zhao, Y. Gao, Z. Chen, Z. Li, T. Ma, Z. Wu, L. Wang, Trifle Pt coupled with NiFe hydroxide synthesized via corrosion engineering to boost the cleavage of water molecule for alkaline water-splitting, Appl. Catal. B Environ. 297 (2021), 120395, https://doi.org/10.1016/j.apcatb.2021.120395.

[37] D.H. Kweon, M.S. Okyay, S.-J. Kim, J.-P. Jeon, H.-J. Noh, N. Park, J. Mahmood, J.-B. Baek, Ruthenium anchored on carbon nanotube electrocatalyst for hydrogen production with enhanced Faradaic efficiency, Nat. Commun. 11 (2020) 1278, https://doi.org/10.1038/s41467-020-15069-3.

[38] J.-S. Li, M.-J. Huang, Y.-W. Zhou, X.-N. Chen, S. Yang, J.-Y. Zhu, G.-D. Liu, L.-J. Ma, S.-H. Cai, J.-Y. Han, RuP2-based hybrids derived from MOFs: highly efficient pH-universal electrocatalysts for the hydrogen evolution reaction, J. Mater. Chem. A 9 (2021) 12276–12282, https://doi.org/10.1039/D1TA01868J.

[39] D. Chen, Z. Pu, R. Lu, P. Ji, P. Wang, J. Zhu, C. Lin, H.-W. Li, X. Zhou, Z. Hu, F. Xia, J. Wu, S. Mu, Ultralow Ru loading transition metal phosphides as high-efficient bifunctional electrocatalyst for a solar-to-hydrogen generation system, Adv. Energy Mater. 10 (2020), 2000814, https://doi.org/10.1002/aenm.202000814.

[40] L. Wang, Q. Zhou, Z. Pu, Q. Zhang, X. Mu, H. Jing, S. Liu, C. Chen, S. Mu, Surface reconstruction engineering of cobalt phosphides by Ru inducement to form hollow Ru-RuP_x-Co_xP pre-electrocatalysts with accelerated oxygen evolution reaction, Nano Energy 53 (2018) 270–276, https://doi.org/10.1016/j.nanoen.2018.08.061.

[41] Q. Qin, H. Jang, L. Chen, G. Nam, X. Liu, J. Cho, Low Loading of Rh_xP and RuP on N, P codoped carbon as two trifunctional electrocatalysts for the oxygen and hydrogen electrode reactions, Adv. Energy Mater. 8 (2018), 1801478, https://doi.org/10.1002/aenm.201801478.

[42] D.R. Liyanage, D. Li, Q.B. Cheek, H. Baydoun, S.L. Brock, Synthesis and oxygen evolution reaction (OER) catalytic performance of $Ni_{2-x}Ru_xP$ nanocrystals: enhancing activity by dilution of the noble metal, J. Mater. Chem. A 5 (2017) 17609–17618, https://doi.org/10.1039/C7TA05353C.

[43] D. Li, X. Chen, Y. Lv, G. Zhang, Y. Huang, W. Liu, Y. Li, R. Chen, C. Nuckolls, H. Ni, An effective hybrid electrocatalyst for the alkaline HER: highly dispersed Pt sites immobilized by a functionalized NiRu-hydroxide, Appl. Catal. B Environ. 269 (2020), 118824, https://doi.org/10.1016/j.apcatb.2020.118824.

[44] S.A. Chala, M.-C. Tsai, W.-N. Su, K.B. Ibrahim, A.D. Duma, M.-H. Yeh, C.-Y. Wen, C.-H. Yu, T.-S. Chan, H. Dai, B.-J. Hwang, Site activity and population engineering of NiRu-layered double hydroxide nanosheets decorated with silver nanoparticles for oxygen evolution and reduction reactions, ACS Catal. 9 (2019) 117–129, https://doi.org/10.1021/acscatal.8b03092.

[45] Y. Liu, X. Liang, L. Gu, Y. Zhang, G.-D. Li, X. Zou, J.-S. Chen, Corrosion engineering towards efficient oxygen evolution electrodes with stable catalytic activity for over 6000 h, Nat. Commun. 9 (2018) 2609, https://doi.org/10.1038/s41467-018-05019-5.

[46] Z. Wu, Y. Zhao, H. Wu, Y. Gao, Z. Chen, W. Jin, J. Wang, T. Ma, L. Wang, Corrosion engineering on iron foam toward efficiently electrocatalytic overall water splitting powered by sustainable energy, Adv. Funct. Mater. 31 (2021), 2010437, https://doi.org/10.1002/adfm.202010437.

[47] H. Sun, W. Zhang, J.-G. Li, Z. Li, X. Ao, K.-H. Xue, K.K. Ostrikov, J. Tang, C. Wang, Rh-engineered ultrathin NiFe-LDH nanosheets enable highly-efficient overall water splitting and urea electrolysis, Appl. Catal. B Environ. 284 (2021), 119740, https://doi.org/10.1016/j.apcatb.2020.119740.

[48] X. Yu, J. Zhao, M. Johnsson, Interfacial engineering of nickel hydroxide on cobalt phosphide for alkaline water electrocatalysis, Adv. Funct. Mater. 31 (2021), 2101578, https://doi.org/10.1002/adfm.202101578.

[49] J. Yu, Q. He, G. Yang, W. Zhou, Z. Shao, M. Ni, Recent advances and prospective in ruthenium-based materials for electrochemical water splitting, ACS Catal. 9 (2019) 9973, https://doi.org/10.1021/acscatal.9b02457.